Low-temperature structural and Raman studies on rare-earth gallates

D. Savytskii, L. Vasylechko,* A. Senyshyn, and A. Matkovskii†
"L'viv Polytechnic" National University, 12 Bandera Street, 79013 Lviv, Ukraine

C. Bähtz
Darmstadt University of Technology, Institute for Materials Science, Petersenstrasse 23, D-64287 Darmstadt, Germany

M. L. Sanjuán
Instituto de Ciencia de Materiales de Aragón (CSIC-UZ), Facultad de Ciencias, Universidad de Zaragoza, 50009 Zaragoza, Spain

U. Bismayer
Mineralogisch-Petrographisches Institut, Universität Hamburg, Grindelallee 48, D-20146 Hamburg, Germany

M. Berkowski
Institute of Physics, Polish Academy of Sciences, Al. Lotników 32/46, 02-668 Warsaw, Poland
(Received 8 October 2002; published 3 July 2003)

Measurements of lattice parameters and structural refinement were made for a $LaGaO_3$, $PrGaO_3$, $NdGaO_3$, $La_{0.34}Pr_{0.33}Nd_{0.33}GaO_3$, and $La_{0.63}Nd_{0.37}GaO_3$ samples by powder-diffraction method using synchrotron radiation. The final structure refinement was performed in space group *Pbnm* at 12 K and room temperature. Anisotropic negative thermal expansion for $PrGaO_3$ samples was detected. Some anomalies of $NdGaO_3$ thermal behavior of lattice parameters were observed. The thermal dependence of the Raman spectra of $NdGaO_3$ single crystals at low temperatures was investigated. Strong interaction of the A_g phonon and the crystal-field excitation of the Nd^{3+} $4f$ electrons of the same symmetry was observed. This leads to a renormalization of the wave function and the energy of the phonon and the crystal-field excitation.

DOI: 10.1103/PhysRevB.68.024101 PACS number(s): 63.20.Kr, 65.40.De, 87.64.Je, 61.10.Nz

I. INTRODUCTION

Perovskite-type gallate compounds $RGaO_3$ have recently been studied because of their wide range of technically attractive properties. For example, single-crystalline neodymium gallate is an excellent substrate material for high-temperature superconductors and doped manganese perovskite $RMnO_3$ films with colossal magnetoresistance.[1,2] The low mismatch between films and substrate lattice parameters and thermal expansion coefficients favors rare-earth gallate substrates. Besides, $NdGaO_3$ single crystals are promising substrate material for GaN film deposition.[3]

The existence of $RGaO_3$ compounds in the R_2O_3-Ga_2O_3 system has first been reported by Geller.[4] Based on x-ray powder-diffraction studies the author stated that the $RGaO_3$ compounds posses an orthorhombically distorted $GdFeO_3$-type structure (space group *Pbnm*) at room temperature. Further structural investigations of these compounds, performed by other research groups, basically confirmed this assumption. On applying different experimental techniques (single-crystal and powder-diffraction, Raman and IR spectroscopy) it was shown that the RT structures of $LaGaO_3$ (Refs. 5–10), $NdGaO_3$ (Refs. 8 and 10–13), and $PrGaO_3$ (Refs. 5 and 14) exhibit centrosymmetric space group *Pbnm*. Modifications of discontinuous solid solutions are found to be formed in $La_{1-x}Pr_xGaO_3$ (Refs. 15 and 16), $La_{1-x}Nd_xGaO_3$ (Refs. 17–19), and $Pr_{1-x}Nd_xGaO_3$ (Ref. 20) pseudobinary systems.

Only a few studies on the low-temperature behavior of the rare-earth (RE) gallates are available up to now. The low-temperature structure of $LaGaO_3$, $NdGaO_3$, and $PrGaO_3$ at 12 K and 298 K was investigated by Marti *et al.*[5] using neutron powder diffraction. It was concluded that there are no phase transitions in this temperature region. Recently, a subtle anomaly near 200 K in the temperature evolution of the dielectric loss angle, magnetic susceptibility, and thermal-expansion coefficient in $NdGaO_3$ single crystals was found.[21] The temperature variations of the integrated intensities of some selected superstructure reflections as well as the crystal structure at 100 K and 293 K based on synchrotron single-crystal diffraction data were examined.[12] No symmetry change, however, could be observed below RT. The temperature anomaly of the physical properties of $NdGaO_3$ seems to be associated with the different character of thermal vibrations of certain cations.[12] In Ref. 22, the specific-heat capacity and the thermal conductivity of substrate-grade $NdGaO_3$ and $LaAlO_3$ single crystals were measured. An anomaly of $Cp(\mathrm{T})$ near $T=12$ K associated with antiferromagnetic ordering of Nd^{3+} cations has been observed.

This work is part of our systematic studies of the structures, optical properties, and phase transitions in RE gallates. In the present paper, we report the thermal-expansion behavior and the crystal structure of $LaGaO_3$, $PrGaO_3$, $NdGaO_3$, and some of their solid solutions ($La_{0.34}Pr_{0.33}Nd_{0.33}GaO_3$, $La_{0.63}Nd_{0.37}GaO_3$) in the temperature range 12–300 K. High-resolution powder-diffraction techniques using synchrotron radiation were applied. Besides, in order to clarify the low-temperature behavior of $NdGaO_3$ Raman-scattering results in the low temperature range are analyzed.

 ©2003 The American Physical Society

II. EXPERIMENTAL DETAILS

$LaGaO_3$, $NdGaO_3$, $La_{0.63}Nd_{0.37}GaO_3$, and $PrGaO_3$ were grown using the Czochralski method, whereas $La_{0.34}Pr_{0.33}Nd_{0.33}GaO_3$ single crystals were grown by the floating-zone technique. The growth procedure has been described in detail in Refs. 11, 19, and 23.

To determine the low-temperature structures of the gallates and their temperature evolution high-resolution synchrotron x-ray-diffraction studies have been performed in the temperature range 12–300 K. Diffraction experiments were carried out using the powder diffractometer at beam line B2 (HASYLAB at DESY) equipped with a He-closed-cycle cryostat. The wavelength was 1.133 40(5) Å (for $LaGaO_3$, $NdGaO_3$, and $La_{0.63}Nd_{0.37}GaO_3$) and 1.124 35(5) Å (for $PrGaO_3$ and $La_{0.34}Pr_{0.33}Nd_{0.33}GaO_3$). In both cases, the wavelength was determined using reflections of a Si standard. To obtain the lattice constants a set of 20 reflections in the 2θ range of 23°–68° was measured for each sample at different temperatures. Full diffraction patterns were collected for $LaGaO_3$, $NdGaO_3$, and $La_{0.63}Nd_{0.37}GaO_3$ at 12 K. All measurements were performed in reflection geometry. Analysis of the data was carried out using the WINCSD program package.[24] Each profile was analyzed using the profile-decomposition program PROFAN in order to obtain the peak position, intensity, and full width at half maximum of every reflection, the number of overlapping peaks and the peak profile. Lattice parameters were refined using the least-square method taking into account a correction of the sample shift. Atomic coordinates and atoms displacement parameters were refined using the full profile Rietveld method. The analysis included the refinement of lattice parameters, positional and displacement parameters, scaling factor, sample shift, background parameter, Bragg-peak profile parameter, and one parameter for the adsorption correction.

A (001)-oriented twin-free $NdGaO_3$ plate with dimensions $2\times2\times1$ mm^3 was used for Raman experiments (Jobin Yvon U1000). Single-crystal Raman spectra were recorded using a charge-coupled device array detector. The exciting radiation was the 514.5 nm line of an argon-ion laser. The light power on the crystal surface was of the order of 20 mW to avoid significant heating, and the spectral resolution was better than 2 cm^{-1}. $z(xx+xy)$-z spectra were recorded at different temperatures in the range 10–300 K. Separate $z(xx)$-z and $z(xy)$-z spectra were measured in a different setup equipped with a diode array detector. The Porto notation $i(jk)l$ is used for the polarization geometry, where i and l denote the direction and j and k the polarization of the incident and scattering light, respectively. The line profiles were fitted to the theoretical spectral function

$$I(I_i^0,\nu_i,\delta_i,\omega)=I_i^0(n(\omega)+1)\omega\delta_i/[(\nu_i^2-\omega^2)^2+\omega^2\delta_i^2], \quad (1)$$

where I_i^0 is a constant, ν_i is the harmonic frequency, δ_i is the damping constant, and $n(\omega)$ is the Bose-Einstein factor. The parameters I_i^0, ν_i, and δ_i were determined by least-squares methods.

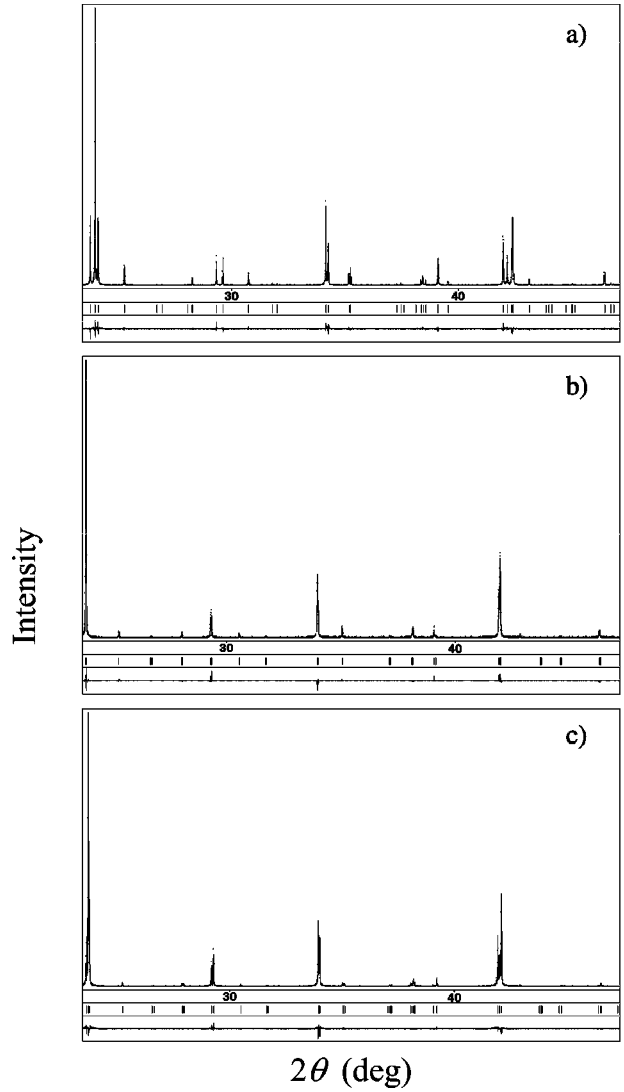

FIG. 1. The graphical result of the Rietvield refinement for $NdGaO_3$ (a), $La_{0.63}Nd_{0.37}GaO_3$ (b), and $LaGaO_3$ (c) structures at 12 K. Parts of the patterns covering the d spacing of 2.75–1.437 Å are shown.

III. RESULTS AND DISCUSSION

A. Low-temperature crystal structure

Taking into account the literature data our previous results of the room-temperature structures of the crystals[8] and the absence of anomalies in the temperature behavior of the lattice constants (see below), the crystal structures of $LaGaO_3$, $La_{0.63}Nd_{0.37}GaO_3$, and $NdGaO_3$ crystals were refined based on the $GdFeO_3$ type. Full-profile Rietveld refinement in the space group *Pbnm* led to a good fit of the calculated and experimental profiles with R_I factors 0.0297, 0.0443, and 0.0487 for $LaGaO_3$, $La_{0.63}Nd_{0.37}GaO_3$, and $NdGaO_3$, respectively. Figure 1 shows the results of our Rietveld refinements. Observed, calculated, I_e-I_c plots and bars indicating positions of the maxima are displayed.

The obtained values of the lattice parameters, positional, and displacement parameters of atoms and final residuals are listed in Table I and the corresponding interatomic distances

TABLE I. Refined structural parameters for $LaGaO_3$, $La_{0.63}Nd_{0.37}GaO_3$, and $NdGaO_3$ at 12 K.

Atom, sites		$LaGaO_3$	$La_{0.63}Nd_{0.37}GaO_3$	$NdGaO_3$
	a Å	5.51395(2)	5.47707(4)	5.41842(2)
	b Å	5.48589(2)	5.48670(4)	5.49534(2)
	c Å	7.76421(3)	7.74500(7)	7.69311(3)
	V Å^3	234.859(3)	232.745(5)	229.070(3)
La (Nd), 4c	x/a	−0.0050(3)	−0.0065(4)	−0.0100(2)
	y/b	0.0200(2)	0.0276(2)	0.0433(1)
	z/c	0.25	0.25	0.25
	B(is/eq)	0.08(2)	0.10(5)	0.10(2)
Ga, 4b	x/a	0.5	0.5	0.5
	y/b	0	0	0
	z/c	0	0	0
	B(is/eq)	0.20(3)	0.40(7)	0.32(4)
O1, 4c	x/a	0.071(2)	0.076(3)	0.088(2)
	y/b	0.487(2)	0.499(2)	0.484(2)
	z/c	0.25	0.25	0.25
	B(is/eq)	0.943	0.669	0.842
O2, 8d	x/a	−0.281(2)	−0.294(2)	−0.2947(13)
	y/b	0.277(2)	0.283(2)	0.2911(13)
	z/c	0.0367(11)	0.0452(15)	0.0432(9)
	B(is/eq)	0.943	0.669	0.842
	R_I	0.0297	0.0443	0.0487
	R_P	0.0935	0.0711	0.1065

and separate angles shown in Table II. The values of the bond-length distortion Δ, for different coordination polyhedra are also given in Table II. Attempts to refine the structures in the noncentrosymmetric space group $Pbn2_1$ or in the monoclinic space group $P2_1/c$ did not lead to improved fits or to a significant decrease of R factors. Hence, the final structure refinement was performed in space group *Pbnm*.

The comparison of the results obtained (Table II) with the RT data[8] show that although all average interatomic distances integrated over all distances in the $RGaO_3$ (R = La, Nd, $La_{0.63}Nd_{0.37}$) structures decrease on decreasing temperature, some individual R-O, Ga-O, and R-Ga lengths show a different behavior. For example, whereas eight nearest R-O distances decrease on cooling, four other distances slightly increase. This indicates that the coordination number 8 should be chosen for the R atoms. Among the six Ga-O distances within the GaO_6 octahedra (Table II) only two decrease on cooling; the distances from the central Ga atom to the four equatorial oxygen atoms remain practically constant. Hence, the GaO_6 octahedra are practically regular in both structures: the bond-length distortions are very small and deviations of O-Ga-O angles from 90° are negligible.

Our analysis shows that similar to the RT structures, all structure deformation parameters, such as the shift of the R cations, the deformation of the R coordination polyhedra, and the tilting degrees of the octahedra increase in the series $LaGaO_3$-$La_{0.63}Nd_{0.37}GaO_3$-$NdGaO_3$. No significant indications for a low-temperature transition were observed in the recorded x-ray-diffraction patterns.

B. Temperature behavior of lattice parameters

The temperature dependencies of the lattice parameters and cell volumes of $LaGaO_3$, $PrGaO_3$, $NdGaO_3$, $La_{0.34}Pr_{0.33}Nd_{0.33}GaO_3$, and $La_{0.63}Nd_{0.37}GaO_3$ crystals are displayed in Fig. 2. Experimental data were fitted by third-order polynomials (Table III). In all compounds the unit-cell changes monotonically with temperature. An anomaly of the lattice parameters is observed for $PrGaO_3$. A minimum is clearly visible in the temperature evolution of the b parameter near 180 K. A similar tendency is observed for the a parameter, but in this case the anomaly is less pronounced and the deviations observed are practically within experimental resolution. The lattice constants of the $La_{0.34}Pr_{0.33}Nd_{0.33}GaO_3$ structure show similar temperature dependence.

Relative thermal expansion of the lattice parameters and cell volume normalized to the data at 12 K is shown in Fig. 3. The relative volume expansions are similar for all crystals. However, for the Pr-containing crystals a somewhat lower relative expansion is observed. An anisotropic behavior of the relative expansion occurs for different crystals. For example, the relative expansions in b direction decrease in the row $LaGaO_3$-$NdGaO_3$-$PrGaO_3$, whereas an opposite behavior is observed in the c direction ($PrGaO_3$-$NdGaO_3$-$LaGaO_3$).

Some anomalies in the temperature behavior of the lattice constants are observed for the $NdGaO_3$ and $PrGaO_3$ crystals. As seen in Fig. 2 changes of the slope of the b parameter occur at temperatures near 50 K and 200 K in $NdGaO_3$.

TABLE II. Selected interatomic distances (in angstrom) in $LaGaO_3$, $NdGaO_3$, and $La_{0.63}Nd_{0.37}GaO_3$ at 12 K.

		$LaGaO_3$	$La_{0.63}Nd_{0.37}GaO_3$	$NdGaO_3$
R–	O1	2.397(11)	2.402(15)	2.328(10)
	2×O2	2.431(10)	2.401(11)	2.373(7)
	O1	2.598(10)	2.523(13)	2.491(10)
	2×O2	2.656(11)	2.583(11)	2.592(7)
	2×O2	2.777(10)	2.792(11)	2.702(7)
	O1	2.953(10)	3.031(13)	3.100(10)
	O1	3.128(11)	3.099(15)	3.126(10)
	2×O2	3.178(10)	3.259(11)	3.333(7)
	$^{a}\Delta BO_8$	3.10214	3.54107	3.103
	ΔBO_9	4.55031	6.23922	7.6144
	ΔBO_{10}	7.04312	8.42677	10.37823
	ΔBO_{12}	10.02588	13.04876	16.78553
Ga–	2×O2	1.962(11)	1.981(11)	1.981(7)
	2×O1	1.982(2)	1.977(3)	1.978(2)
	2×O2	1.995(11)	1.985(11)	1.984(7)
	ΔBO_6	0.04701	0.00272	0.00153
R–	2×Ga1	3.2713(7)	3.2204(9)	3.1620(6)
	2×Ga1	3.351(1)	3.327(2)	3.286(1)
	2×Ga1	3.396(2)	3.390(2)	3.376(1)
	2×Ga1	3.4507(7)	3.4987(9)	3.5523(6)
R-	2×R	3.850(2)	3.823(2)	3.782(1)
	2×R	3.8887(1)	3.8883(2)	3.8776(1)
	2×R	3.928(2)	3.931(2)	3.937(1)
Ga-	2×Ga1	3.8821(1)	3.8726(1)	3.8473(1)
	4×Ga1	3.8892(1)	3.8762(1)	3.8591(1)
O1–	2×O2	2.778(12)	2.74(2)	2.798(9)
	2×O2	2.799(13)	2.77(2)	2.799(10)
	2×O2	2.802(14)	2.823(13)	2.800(9)
	2×O2	2.821(12)	2.862(14)	2.806(10)
O2-	2×O2	2.76(2)	2.76(2)	2.785(10)
	2×O2	2.83(2)	2.84(2)	2.822(10)
aGa1..O1..bGa1		156.7(5)	156.8(7)	152.9(4)
aGa1..O2..bGa1		158.8(6)	155.5(6)	153.4(4)

[a] Δ are defined as $1/n\Sigma\{(r_i-r)/r\}^2\times10^3$.

Negative thermal expansion along the *b* direction is evident in $PrGaO_3$. No visible anomalies are observed in the temperature behavior of the lattice constants of $LaGaO_3$ and $La_{0.63}Nd_{0.37}GaO_3$. The difference between the two groups of crystals may be explained by the presence of the R^{3+} cations with $4f$ electrons in $NdGaO_3$, $PrGaO_3$, and $La_{0.34}Pr_{0.33}Nd_{0.33}GaO_3$ crystals and the absence (or low concentration) of such ions in case of $LaGaO_3$ and $La_{0.63}Nd_{0.37}GaO_3$.

The observed anomalies in the temperature behavior of the lattice parameters in $PrGaO_3$ and $NdGaO_3$ can be explained as follows. An important feature of the studied framework structures is the rotational vibration of the shared polyhedra (in the perovskite structure—anion octahedra). Some of these vibrations are related to soft modes for the rotational phase transitions. Since rotational modes will have a negative contribution to the thermal expansion, they significantly counteract to other modes that induce expansions of the bondings and hence, lead to positive thermal expansion. Whether the combination leads to negative thermal expansion or a phase transition depends on how significant fractions of vibrations involve modes that are related to rotations of octahedra.[25] Moreover, many modes will involve a mixture of rotations and distortions of oxygen octahedra and the balance will depend on details of the crystal structure, in particular, on interactions between crystal vibrations and electronic excitations of R^{3+} ions in perovskites containing such rare-earth ions.

As demonstrated in Ref. 26 and 27 coupling between the low-lying Pr^{3+} electronic levels and the phonon modes corresponding to staggered rotations of the AlO_6^{3-} octahedra led to the two additional phase transitions below room temperature in the structurally related $PrAlO_3$ perovskite. $NdAlO_3$ does not undergo any additional phase transition (magnetic or structural) down to 2 K, nevertheless, according to the data of Ref. 28 a pronounced ion-phonon interaction for the $^4I_{9/2}$ ground multiplet of Nd^{3+} is observed.

C. Temperature dependence of Raman spectra in $NdGaO_3$

Similar to aluminates, rare-earth ion-phonon interactions may be expected in corresponding gallates. The temperature behavior of the Raman spectra allows to obtain information on such interactions.[29,30] Studies were performed only on $NdGaO_3$ single crystals as strong twinning occurs in the other rare-earth gallates which hinders quantitative measurements of polarized Raman-scattering spectra.

Factor-group analysis shows that excitations of crystals of the ABO_3 type with space group *Pbnm* and four formula units per unit cell are (Ref. 10)

$$\Gamma_{opt}=7A_g(r)+7B_{1g}(r)+5B_{2g}(r)+5B_{3g}(r)+8A_u(n)$$
$$+7B_{1u}(ir)+9B_{2u}(ir)+9B_{3u}(ir),$$

$$\Gamma_{ac}=B_{1u}+B_{2u}+B_{3u}, \tag{2}$$

with r—raman active modes, ir—IR active modes and n—silent modes.

Polarized low-temperature spectra in xx and xy geometries are shown in Fig. 4(a). The polarization properties of these spectra allow us to separate some close modes and to assign A_g and B_{1g} phonons unambiguously. In the xx spectrum, we observe excitations at 87.5, 104.4, 147.8, 184, 217.7, 295.7, 342.6, and 472.3 cm^{-1}, while in xy we find bands at 90.3, 155.1, 184.4, 219.9, 364.8, and 454.2 cm^{-1}. The relation of some of these frequencies to those of phonons at RT (Refs. 10, 13, and 31) allows us to assign peaks at 147.8, 217.7, 295.7, 342.6, and 472.3 cm^{-1} in xx to A_g phonons and peaks at 155.1, 219.9, 364.8, and 454.2 cm^{-1} in xy to B_{1g} phonons. This agrees well with the values given in Ref. 31 for low-*T* phonons. The band at 184 cm^{-1} is correlated with a crystal-field (CF) transition.[31] In the range 80–120 cm^{-1} some peaks appear at low temperatures. While only one mode is observed at RT (the A_g at 95 cm^{-1}), two bands are observed in the xx spectrum at 12 K (at 87.5 and 104.4 cm^{-1}) and one more in xy (at 90.3 cm^{-1}). In Fig. 4(b), we show the temperature evolution

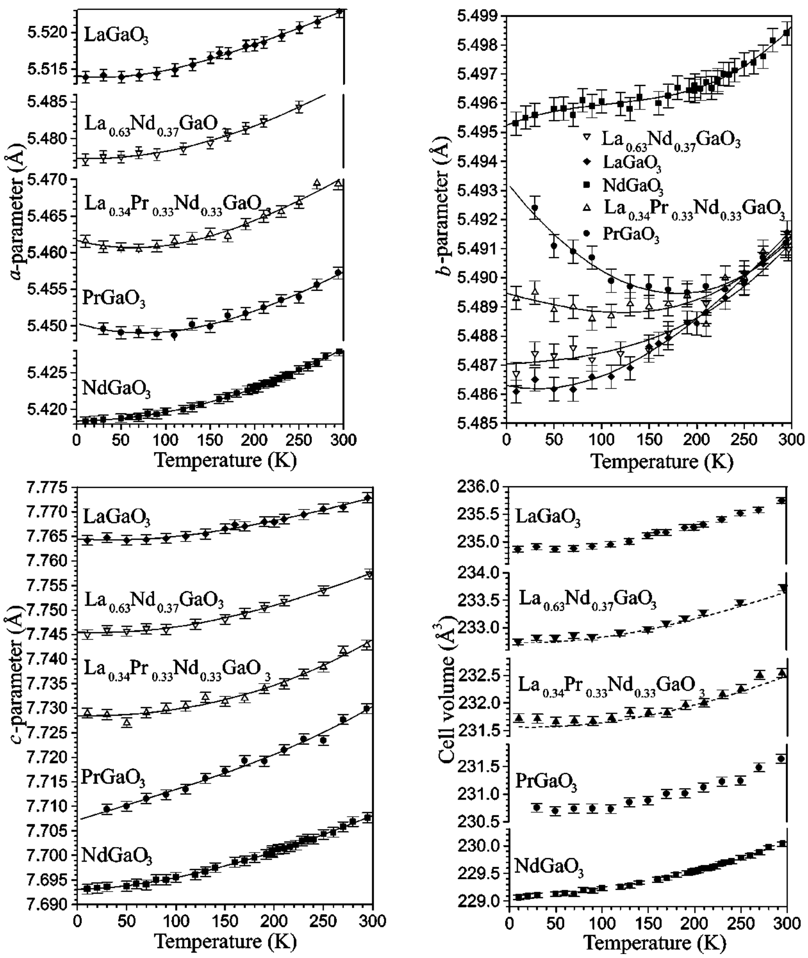

FIG. 2. Temperature evolution of the lattice parameters and cell volume (∇, $La_{0.63}Nd_{0.37}GaO_3$; $\Diamond$, $LaGaO_3$; $\blacksquare$, $NdGaO_3$; Δ, $La_{0.34}Pr_{0.33}Nd_{0.33}GaO_3$; $\bigcirc$, $PrGaO_3$). Experimental points were fitted by third-order polynomials (solid lines). The dashed lines of the $V(T)$ graph illustrate the behavior of the cell volumes, estimated from Vegard's rule, the solid line—results from third polynomial fitting.

of the low-frequency region of the spectrum from 10 to 300 K. The temperature dependence of the Raman shifts of the bands are shown in Fig. 5. The continuity of the band at 104 cm^{-1} at low temperatures with the 95 cm^{-1} phonon at RT suggests that it is related to the same A_g phonon. On the other hand, the bands close to 90 cm^{-1}, seen only at low temperature, have an energy close to that of the first excited state of Nd^{3+} ions, as reported in the literature.[13,32] It is therefore plausible to assign these two bands to the CF transitions from the ground to the first exctited state.

In general the frequency of all normal modes change depending on the cell volume according to

$$\frac{\nu_j}{\nu_j^0}=\left(\frac{V^0}{V}\right)^{\gamma}, \tag{3}$$

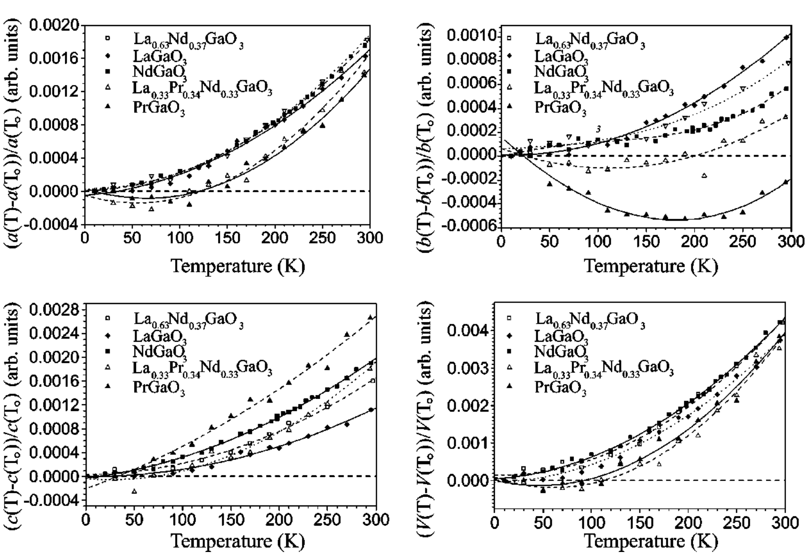

FIG. 3. Relative thermal expansion of the lattice parameters and cell volume, normalized to the data at $T_0 = 12$ K.

TABLE III. The results of polynomial fitting ($A+BT+CT^2+DT^3$) of the lattice parameters and cell volume in temperature range 12–300 K.

	a, Å	b, Å	c, Å	V, Å ^{3}
		$LaGaO_3$		
A	5.51352	5.48601	7.76372	234.8436
$B\times10^{-6}$	1.11013	0.26777	6.96274	−62.9674
$C\times10^{-7}$	1.42147	6.32997	0.69300	130.811
$D\times10^{-10}$	−1.33103	−2.90328	0.37448	−89.0872
R(COD)	0.99817	0.98926	0.98076	0.99079
		$La_{0.63}Nd_{0.37}GaO_3$		
A	5.47689	5.48681	7.74496	232.73984
$B\times10^{-6}$	6.08242	7.78623	5.62937	785.277
$C\times10^{-7}$	0.768406	0.290573	1.14781	52.8531
$D\times10^{-10}$	0.648945	1.7489	0.282874	114.731
R(COD)	0.99358	0.96008	0.9925	0.98969
		$NdGaO_3$		
A	5.4184	5.49525	7.6931	229.06476
$B\times10^{-6}$	2.66446	13.2442	6.00976	887.745
$C\times10^{-7}$	0.945108	−0.908162	1.92338	55.6518
$D\times10^{-10}$	0.221865	2.80669	-1.49942	90.5691
R(COD)	0.9991	0.9748	0.99819	0.99815
		$La_{0.34}Pr_{0.33}Nd_{0.33}GaO_3$		
A	5.4617	5.48948	7.72848	231.74352
$B\times10^{-6}$	−33.0515	−9.07556	−2.41324	−1940
$C\times10^{-7}$	2.87204	0.13898	1.41626	1576.99
$D\times10^{-10}$	−2.71723	1.27767	1.28827	19.4761
R(COD)	0.97833	0.81923	0.97705	0.98039
		$PrGaO_3$		
A	5.45039	5.49328	7.70713	230.75506
$B\times10^{-6}$	−37.9438	−40.7577	64.7366	−1380
$C\times10^{-7}$	2.85228	0.996676	−0.453591	148.704
$D\times10^{-10}$	−2.71537	0.494775	2.93639	−5.065
R(COD)	0.9839	0.94637	0.98933	0.98506

where ν_j is the frequency when the volume is equal to V, ν_j^0 is the frequency when the volume is V^0 and γ is the Gruneisen parameter. To clarify the temperature behavior of phonon vibrations, we calculated the Gruneisen parameter for the observed modes. The temperature dependence of the Gruneisen parameters γ_i for the observed modes ν_j in the Raman spectra is shown in Fig. 6. Both frequency and volume were normalized to the values at room temperature and the Gruneisen parameters γ_i were calculated according to

$$\gamma_i=\ln(\nu_j/\nu_j^{300})/\ln(V^{300}/V). \quad (4)$$

The values of the parameters γ_i of the four strongest modes are of the order of 5–7 and are virtually thermally independent (Fig. 6). The phonon vibration at 144 cm^{-1} is weak [Fig. 4(b)] and has not been analyzed due to the uncertainty in the determination of the band position. As shown in Fig. 6, a strong temperature dependency of the low-energy phonon (95 cm^{-1} at RT) is observed that can be correlated with the electron-phonon coupling. The temperature behavior of the unrenormalized frequency of the phonon (Fig. 5, curve 3) was determined using Eq. (4) and the average Gruneisen parameter at each temperature (Fig. 6, solid line). At 10 K a difference between values of observed and calculated unrenormalized frequencies of the low-energy phonon mounts to 7 cm^{-1} (Fig. 5, curves 4 and 3 correspondingly).

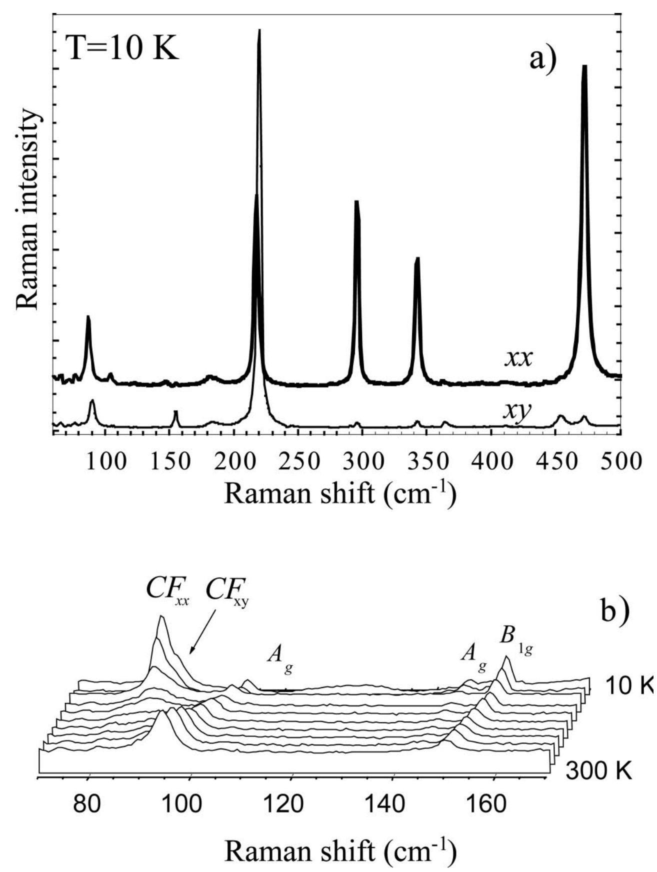

FIG. 4. The low-temperature polarized Raman spectra of $NdGaO_3$ single crystals in xx and xy geometries (a) and the temperature evolution of the low-frequency region of the spectrum from 10 to 300 K in ($xx+xy$) scattering geometry (b).

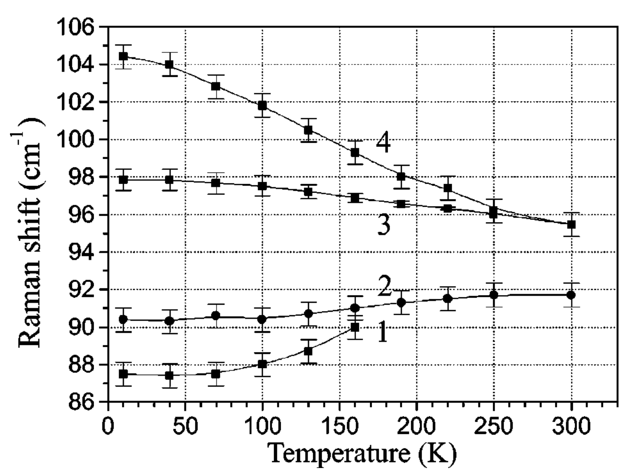

FIG. 5. Thermal evolution of the crystal-field excitation (CFE) of the A_g (1) and B_{1g} (2) modes and the unrenormalized (3) and experimental (4) frequency of the A_g phonon in the $NdGaO_3$ single crystal.

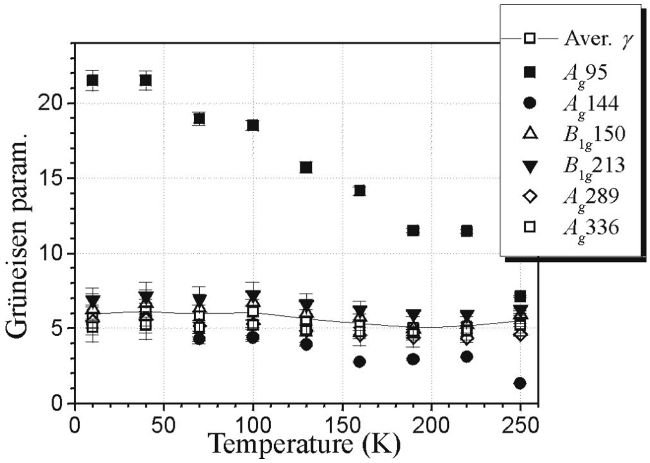

FIG. 6. Temperature dependencies of the Gruneisen parameters γ_i for observed modes ν_i (95, 144, 150, 213, 289, 336 cm^{-1}) in the Raman spectra and the average Gruneisen parameter for four strong modes 150, 213, 289, 336 cm^{-1} in the $NdGaO_3$ crystal.

The ground state of the $4f^3$ configuration of free Nd^{3+} ions is $^4I_{9/2}$. In our case, the crystal symmetry is orthorhombic ($Pbnm$ or D_{2h}^{16}) with Nd ions on a site of C_s symmetry, and the $^4I_{9/2}$ multiplet splits into five $\Gamma_3+\Gamma_4$ Kramers doublets. However, since we shall consider coupling of the crystal-field transition (CFT) to lattice phonons, the correlation of Nd levels to the lattice symmetry D_{2h} yields five Γ_6 Kramers doublets. Transitions between them will be governed by selection rules according to the result of the direct product of initial- and final-state representations:

$$\Gamma_6 \times \Gamma_6 = A_g + B_{1g} + B_{2g} + B_{3g} . \quad (5)$$

In $NdGaO_3$, only Nd and O atoms lead to Raman-active excitations. They can both contribute to A_g modes, though the low-frequency A_g mode close to 100 cm^{-1} is likely to involve mostly Nd vibrations. The vibration of either Nd alone (or Nd plus oxygen) results in a modulation of the CF potential at the Nd site and thus, affects the electronic levels of Nd ions, which allows for a coupling between phonons and CF excitations, provided they have the same symmetry and close enough energies. These conditions are fulfilled by the A_g phonon and the A_g channel of the CF transition to the first excited state which will be seen in xx, yy, or zz geometries. Therefore, a coupling is expected in these configurations, producing a renormalization of CF and phonon energies. On the contrary, no coupling is expected in xy geometry, since the phonon is forbidden in this configuration. Hence, the position of the CF transition in the xy spectrum gives the unrenormalized value of the CFT energy. Within this model, the temperature evolution of the Raman shifts in xx geometry (~ 3 cm^{-1} at 10 K), shown in Fig. 5, are interpreted as the result of the coupling strength decreasing with increasing temperature. This has usually been observed in coupled modes of high-T_c superconductors.[29,30]

At nonzero temperature, all CF levels of the Nd^{3+} ions are occupied according to Boltzmann statistics.[29] The temperature evolution of the level populations of the $^4I_{9/2}$ term in $NdGaO_3$ is shown in Fig. 7. The energy of the next-higher term $^4I_{11/2}$ is about 2000 cm^{-1} higher and thus these levels were not taken into account in the calculation of the populations of the $^4I_{9/2}$ levels. The coupling is proportional to the difference in the population between the two levels contributing to the crystal-field excitation.[33] As shown by our calculation (Fig. 7), the difference in the population between first and second level is near $0.2\times N$ at 250 K and increases rapidly with decreasing temperature with N being the number of unit cells in the crystal. This may explain the disappearance of the coupling on increasing temperature.

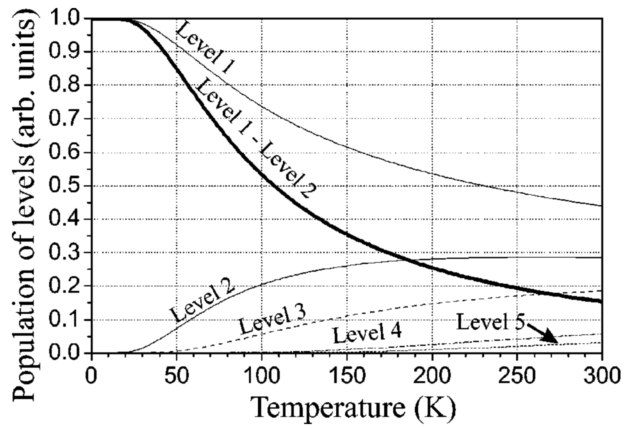

FIG. 7. Thermal evolution of the level populations of the $^4I_{9/2}$ term and population difference between the two levels contributing to the crystal-field excitation in the $NdGaO_3$ single crystal.

IV. CONCLUSION

La, Nd gallates do not undergo any phase transition (magnetic or structural) down to 12 K. Nevertheless, from our Raman spectra, it was concluded that there is interaction of the A_g phonon and the crystal-field excitation of the $^4I_{9/2}$ ground multiplet of the Nd^{3+} ion, which is, however, insufficient to induce a phase transformation in $NdGaO_3$, but is enough to cause anomalies of the thermal expansion. Negative thermal expansion in b direction below 160 K was observed in $PrGaO_3$, which can also be attributed to an interaction between the phonon vibrations and the electronic excitations of the Pr ion. Further studies on this anomaly are in progress.

ACKNOWLEDGMENTS

The authors acknowledge Dr. B. Güttler's help with Raman investigations. The work was supported by WTZ (UKR 01/12), Ukrainian Ministry of Science (Project No. 2M/1856-97), Polish Committee for Scientific Research (Grant No. N 7 T08A 00520), Spanish CICYT under Project No. MAT2001-3713-C04-02, and ICDD Grant-in-aid program. A.S. gratefully acknowledges the financial support of the Deutscher Akademischer Austauschdienst (Leonhard—Euler program). L.V. acknowledges the Max-Planck Society. M.L.S. thanks Dr. V. M. Orera and Dr. R. I. Merino for fruitful discussions on Raman and optical spectroscopy of rare-earth gallates.

*Corresponding author. Also at Max-Planck-Institut für Chemische Physik fester Stoffe, Nöthnitzerstrasse 40, D-01187 Dresden, Germany. Email address: crystal@polynet.lviv.ua
†Also at: Institute of Physics, University of Rzeszów, Rejtana 16a, 35-310 Rzeszów, Poland.

[1] A. Mogro-Campero, L.G. Turner, E.L. Hall, M.I. Garbauskas, and N. Lewis, Appl. Phys. Lett. **54**, 2719 (1989).
[2] R.L. Sandstrom, E.A. Giess, W.J. Gallagher, A. Segmuller, E.I. Cooper, M.F. Chisholm, A. Gupta, S. Shinole, and R.B. Laibowitz, Appl. Phys. Lett. **53**, 1874 (1988).
[3] V.V. Mamutin, A.A. Toropov, N.F. Kartenko, S.V. Ivanov, A. Wagner, and B. Monemar, Mater. Sci. Eng. **59**, 56 (1999).
[4] S. Geller, Acta Crystallogr. **10**, 243 (1957).
[5] W. Marti, P. Fischer, F. Altorfer, H. Scheel, and M. Tadin, J. Phys.: Condens. Matter **6**, 127 (1994).
[6] M. Lerch, H. Boysen, and T. Hansen, J. Phys. Chem. Solids **62**, 445 (2001).
[7] C. Howard and B. Kennedy, J. Phys.: Condens. Matter **11**, 3229 (1999)
[8] L. Vasylechko, A. Matkovskii, D. Savytskii, A. Suchocki, and F. Wallrafen, J. Alloys Compd. **292**, 57 (1999).
[9] P.R. Slater, J.T.S. Irvine, T. Ishibara, and Y. Rakita, J. Solid State Chem. **139**, 135 (1998).
[10] M.L. Sanjuan, V.M. Orera, R.I. Merino, and J. Blasco, J. Phys.: Condens. Matter **10**, 11 687 (1998).
[11] S. Ubizskii, L. Vasylechko, D. Savytskii, A. Matkovskii, and I. Syvorotka, Supercond. Sci. Technol. **7**, 766 (1994).
[12] L. Vasylechko, L. Akselrud, W. Morgenroth, U. Bismayer, A. Matkovskii, and D. Savytskii, J. Alloys Compd. **297**, 46 (2000).
[13] D.I. Savytskii, D.Yu. Sugak, A.O. Matkovskii, A. Suchocki, I.V. Savytskii, V.I. Dzhala, and P. Kaczor, Proc. SPIE **283**, 3178 (1997).
[14] L. Vasylechko, D. Savytskii, H. Schmidt, U. Bismayer, A. Matkovskii, and M. Berkowski, Hasylab Annual Report **1**, 2764 (2000).
[15] P. Byszewski, E. Kowalska, R. Diduszko, R. Aleksiyko, M. Berkowski, J. Fink-Finowicki, and J. Kapusniak, J. Therm Anal. Calorim. **65**, 545 (2001).
[16] L. Vasylechko, Visnyk Lviv. Univ., Ser. Khim. **40**, 98 (2001).
[17] L. Vasylechko, M. Berkowski, A. Matkovskii, W. Piekarczyk, and D. Savytskii, J. Alloys Compd. **300–301**, 471 (2000).
[18] L. Vasylechko, M. Berkowski, A. Matkovski, D. Savytskii, and J. Fink-Finowicki, Mater. Res. Bull. **35**, 333 (2000).
[19] M. Berkowski, J. Fink-Finowicki, W. Piekarczyk, L. Perchuc, P. Byszewski, L.O. Vasylechko, D.I. Savytskii, K. Mazur, J. Sass, E. Kowalska, and J. Kapusniak, J. Cryst. Growth **209**, 75 (2000).
[20] R. Aleksiyko, M. Berkowski, P. Byzhewski, B. Dabrowski, R. Diduszko, J. Fink-Finowicki, and L.O. Vasylechko, Cryst. Res. Technol. **36**, 789 (2001).
[21] D. Savytskii, S. Ubizskii, A. Matkovskii, A. Suchocki, U. Bismayer, V. Pashkov, V. Borisov, A. Alexandrovskii, and A. Soldatov, Phase Transitions **70**, 57 (1998).
[22] W. Schnelle, R. Fischer, and E. Gmelin, J. Phys. D **34**, 846 (2001).
[23] M. Berkowski, J. Fink-Finowicki, P. Byszewski, R. Diduszko, E. Kowalska, R. Aleksiyko, W. Piekarczyk, L.O. Vasylechko, D.I. Savytskii, L. Perhuc, and J. Kapusniak, J. Cryst. Growth **222**, 194 (2001).
[24] L.G. Akselrud, P.Yu. Zavalij, Yu. Grin, V.K. Pecharsky, B. Baumgartner, and E. Woelfel, Mater. Sci. Forum **133-136**, 335 (1993).
[25] A.K.A. Pryde, K.D. Hammonds, M.T. Dove, V. Heine, J.D. Gale, and M.C. Warren, J. Phys.: Condens. Matter **8**, 10973 (1996).
[26] K.B. Lyons, R.J. Birgeneau, E.I. Blount, and L.G. Van Uitert, Phys. Rev. B **11**, 891 (1975).
[27] S.M. Moussa, B.J. Kennedy, B.A. Hunter, C.J. Howard, and T. Vogt, J. Phys.: Condens. Matter **13**, L203 (2001).
[28] E. Finkman, E. Cohen, and L.G. Van Uitert, Phys. Rev. B **7**, 2899 (1973).
[29] E.T. Heyen, R. Wegerer, E. Schonherr, and M. Cardona, Phys. Rev. B **44**, 10 195 (1991).
[30] T. Ruf, Physica B **219-220**, 132 (1996).
[31] O. Kamishima, H. Koyama, R. Takahashi, Y. Abe, T. Sato, and T. Hattori, J. Phys.: Condens. Matter **14**, 3905 (2002).
[32] A. Podlesnyak, S. Rosenkranz, F. Fauth, W. Marti, A. Furrer, A. Mirmelstein, and H.J. Scheel, J. Phys.: Condens. Matter **5**, 8973 (1993).
[33] P. Thalmeier and P. Fulde, Phys. Rev. Lett. **49**, 1588 (1982).